ACS OMEGA

Open Access

http://pubs.acs.org/journal/acsodf

Article

Synthesis of Symmetrical Silane Containing P═O Bonds and Their Passivation of Perovskites

Baoyang Dai, Shanshan Yan, Zhimi Chen, Tucai Zheng, Jie Qin, Junhua Zhao, Wanting Jin, Chunhui Zhou, Li Wan, Xing Su, and Chuanhua Gao*

Cite This: *ACS Omega* 2025, 10, 3486−3493

Read Online

ACCESS | Metrics & More | Article Recommendations | Supporting Information

ABSTRACT: Perovskite quantum dots (QDs) exhibit unique advantages, including a wide color gamut, narrow full width at half-maximum, cost-effectiveness, and high-efficiency luminescence, positioning them as a significant focus in contemporary optoelectronic research. Nevertheless, the synthesis of QDs often introduces crystal defects, while conventional in situ ligands can detrimentally affect the optoelectronic properties of perovskites. To overcome these challenges, we synthesized a symmetrical silane-based passivating agent containing phosphorus−oxygen double bonds. This agent enabled the in situ passivation of perovskites, significantly improving their optical performance and stability. Results showed that postpassivation QDs demonstrated bright green photoluminescence (PL) at 525 nm, with a 28% enhancement in PL intensity, a 16% increase in photoluminescence quantum yield, and an average lifetime (τ_{ave}) extended by 191.2 ns. Furthermore, the thermal stability at 80 °C improved by 3.75-fold, and the stability under 84% relative humidity conditions increased by 21%. 1,3-bis(3-diethoxyphosphorylpropyl)-1,1,3,3-tetramethyldisiloxane (SPE)-passivated perovskites are viable for practical applications.

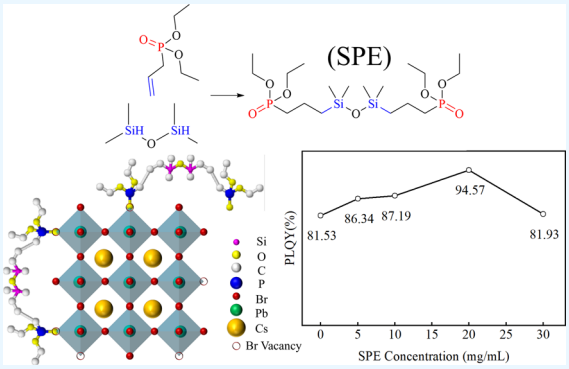

1. INTRODUCTION

Perovskite materials, due to their outstanding optoelectronic properties, have become a key focus of research on novel optoelectronic devices, such as light-emitting diodes and solar cells.[1−6] However, the practical applications of perovskite materials face critical challenges, such as inadequate material stability and short device lifetimes.[5,7] In recent years, surface and interface passivation of perovskite materials have emerged as an important strategy to enhance device performance and stability.[8,9]

Currently, passivating agents for perovskite materials fall into three main categories: inorganic passivating agents,[10−14] organic passivating agents,[15−18] and polymers.[19−22] Inorganic passivating agents typically employ charged ions to form ionic bonds at perovskite defect sites, thereby optimizing the crystal structure. Organic passivating agents are typically big molecules with specific functional groups that interact with the surface defects of perovskites, effectively regulating perovskite crystallization. Similarly, polymers feature long, ordered molecular structures that promote sustained defect passivation.

Among these, phosphorus-containing compounds have garnered significant attention as a distinct and effective class of passivating agents.[5,23−25] Phosphorus exhibits excellent coordination capabilities and electron affinity, enabling the effective passivation of defect sites in perovskite materials. This suppression of carrier recombination and ion migration enhances the efficiency of luminescence and the stability of the material.[26] For instance, Bao et al.[27] reported the use of a phosphorus-containing polymer as a passivation layer, achieving an external quantum efficiency of up to 20% and a light-emitting diode lifetime exceeding 800 h. In a similar study, Cheng et al.[28] employed diphenylphosphine oxide (DPPO), a compound containing two phosphine oxide groups, to passivate Pb^{2+} defects in perovskite crystals. The DPPO adjusted the energy level alignment of the perovskite, improved carrier transport efficiency, and reduced nonradiative recombination. As a result, the power conversion efficiency reached 24.24%.

Despite significant advancements, the optimization of the molecular structure of phosphorus-containing passivating agents, the diversification of the types of passivating agents, and the elucidation of the passivation mechanisms to achieve high-performance and long-term stability of perovskite optoelectronic devices remain critical scientific challenges in

Received: August 16, 2024
Revised: January 4, 2025
Accepted: January 10, 2025
Published: January 24, 2025

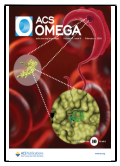

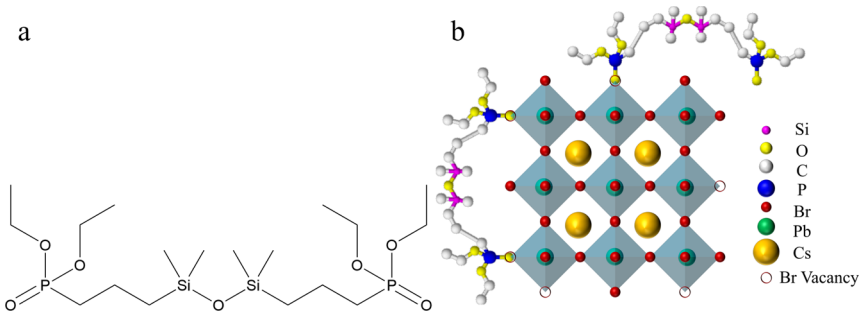

Figure 1. (a) Schematic diagram of the SPE structure. (b) Schematic diagram of the SPE passivation.

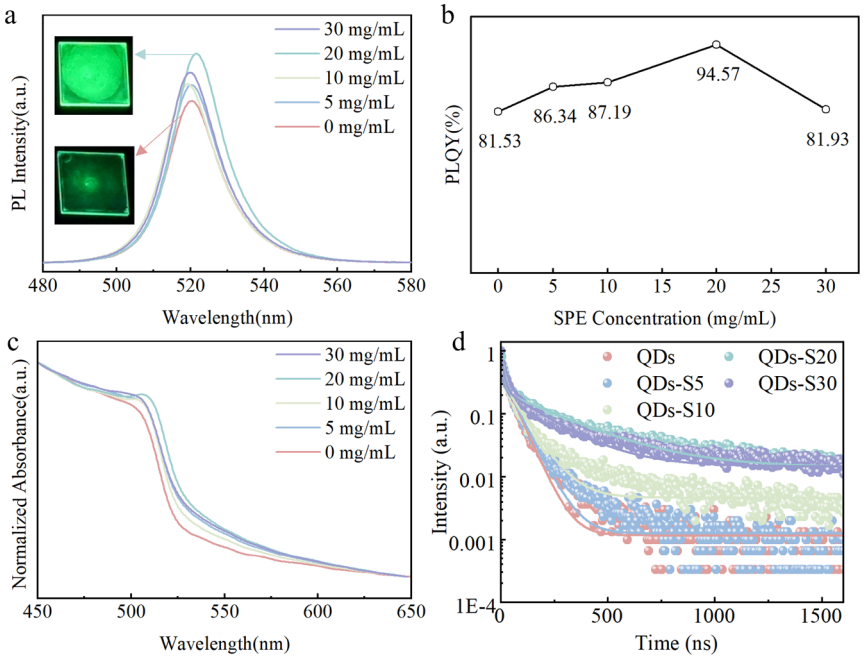

Figure 2. (a–c) PL, PLQY, and UV–vis absorption spectra of perovskites before and after passivation as a function of the SPE concentration. (d) TRPL spectra of QDs, QDs-S5, QDs-S10, QDs-S20, and QDS-S30.

this field.[29−31] In this study, a silane compound with a symmetrical structure incorporating phosphorus−oxygen double bonds was synthesized to modify perovskite materials. A systematic investigation into the passivation mechanisms of this compound was undertaken to provide valuable insights that would advance perovskite material development and promote practical breakthroughs in the emerging field of optoelectronics.

2. RESULTS AND DISCUSSION

Figure S1 illustrates the reaction mechanism for the synthesis of SPE. Figure S2 presents the phosphorus nuclear magnetic resonance (NMR) spectra of diethyl allyl phosphate (DAPP) and SPE, revealing a chemical shift change from 27.53 to 32.35 ppm. This shift is indicative of the complete reaction of DAPP, resulting in the formation of the new substance SPE. As shown in Figure 1a, the phosphorus and oxygen atoms in the passivating agent SPE molecule exhibit strong electronegativity. The phosphorus−oxygen double bond (P═O) functions as an electron-withdrawing group. During the synthesis of perovskites using a precursor solution containing the SPE passivating agent, the P═O group occupies Br^- ion vacancies in the perovskite lattice, coordinating with Pb^{2+} ions and enhancing the crystal structure (Figure 1b).[5,32,33]

The Si−O−Si structure within the SPE molecule provides hydrophobicity to the perovskite material. The carbon−oxygen-silicon bonds in the main chain exhibit high bond energies, contributing to excellent chemical stability. Furthermore, the silicon atom (1.17 Å) exhibits a significantly larger size compared with the carbon atom (0.77 Å), resulting in the formation of stronger van der Waals forces between molecules. The alkyl side chains, being nonpolar, render the entire molecular chain nonpolar and hydrophobic. Consequently, SPE not only optimizes the crystal structure of the perovskite but also enhances its hydrophobicity, thereby improving the optical properties and stability of the perovskite material.

2.1. Optical Properties of $CsPbBr_3$. As shown in Figure 2, the optical properties of QDs were characterized by using photoluminescence (PL) spectra, photoluminescence quantum yield (PLQY), and UV−vis absorption spectra. As depicted in Figure 2a, it was observed that, in comparison to unpassivated perovskites, the PL intensity of passivated perovskites exhibited an initial increase, followed by a subsequent decrease with increasing concentrations of the SPE passivating agent. At a concentration of 20 mg/mL of the SPE passivating agent, the PL intensity of the perovskites reaches its maximum, showing a 28% increase compared to unpassivated perovskites, accom-

https://doi.org/10.1021/acsomega.4c07572
ACS Omega 2025, 10, 3486−3493

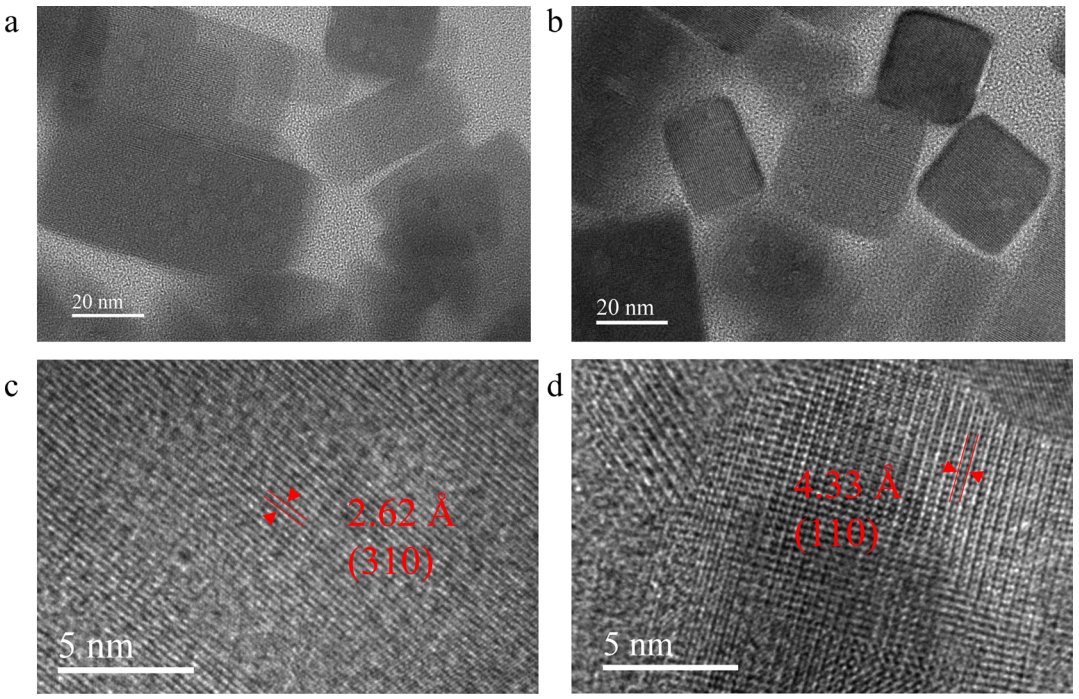

Figure 3. (a, b) TEM images of the QDs and QDs-S20, respectively. (c, d) HRTEM images of the QDs and QDs-S20, respectively.

panied by a slight shift toward higher wavelengths. The substantial enhancement in PL intensity postpassivation is attributed to the SPE passivating agent enhancing the crystal structure of the perovskites and suppressing nonradiative recombination, thereby enhancing their optical properties. However, it is noteworthy that an excess of SPE leads to a decline in PL intensity, attributable to the surplus passivating agent exerting an adverse effect on the photon transmission process within the perovskites. Furthermore, the pale yellow color of the SPE solution can absorb transmitted photons, thereby further diminishing the PL intensity.

Figure 2b presents the PLQY results of perovskites before and after SPE passivation. The PLQY of the unpassivated perovskites is 81.53%, which increases to 94.57% after SPE passivation. This enhancement in PLQY is consistent with the trend observed in PL intensity, suggesting that the optimal passivation effect is achieved at a 20 mg/mL concentration of SPE. Beyond this concentration, a precipitous decline in PLQY is observed, suggesting that the color of the passivating agent exerts a more substantial influence on the PLQY value at higher concentrations.

As illustrated in Figure 2c, the absorption spectra of the perovskites were examined before and after SPE passivation. The position of the absorption peak remains relatively constant at approximately 506 nm, indicating that the SPE passivating agent effectively passivates crystal defects without altering the overall crystal structure.[34]

Urbach energy (Eu) is a common tool used to evaluate the degree of disorder in perovskites.[35−37] In this study, Eu was calculated from the perovskite absorption data (Figure S3a−e),[38] and the results are shown in Figure S3f, for comparing structural disorder in perovskites. A comparison of unpassivated perovskites and perovskites passivated with SPE reveals an initial decrease in the amount of Eu, followed by a slight increase. The Eu of unpassivated perovskites is 19.98 meV, while at an SPE concentration of 20 mg/mL, it decreases to 16.86 meV, representing a reduction of 3.12 meV. This reduction indicates that the SPE passivating agent enhances the crystalline arrangement and structural integrity of the perovskites. However, at concentrations exceeding 20 mg/mL, the Eu value slightly increases, though it remains lower than that of unpassivated QDs. Collectively, these observations suggest that the incorporation of SPE leads to a reduction in defect density within perovskites, in comparison to unpassivated QDs, thereby enhancing their optoelectronic performance.

Time-resolved photoluminescence (TRPL) data were analyzed through the implementation of a biexponential eq 1, thereby yielding the calculation of the average carrier lifetime (τ_{ave}) in accordance with eq 2.[39] Within the framework of this model, τ_1 and τ_2 denote the fast and slow decay lifetimes, respectively, thereby reflecting the radiative and nonradiative recombination processes. A_1 and A_2 represent the relative amplitudes of these decay components. As demonstrated in Figure 2d and Table S1, the average carrier lifetime (τ_{ave}) of the perovskites exhibited an increase from 48.01 ns (QDs) to 239.21 ns (QDs-S20) as the SPE concentration increased, while τ_{ave} decreased from 239.21 ns (QDs-S20) to 158.93 ns (QDs-S30) as the SPE concentration continued to increase. The findings suggest that the interaction between SPE and perovskites initially enhances the average carrier lifetime by effectively passivating defects in the perovskite material. This, in turn, reduces nonradiative recombination and improves the crystal structure. Conversely, an excess of SPE has been shown to exert a contradictory effect, which can likely be attributed to overloading.[40] This outcome aligns with the previously discussed findings, thereby further demonstrating the superior ability of SPE molecules to effectively passivate perovskites.

$$I(t) = A_1\exp(-t/\tau_1) + A_2\exp(-t/\tau_2) \quad (1)$$

$$\tau_{ave} = (A_1\tau_1^{\,2} + A_2\tau_2^{\,2})/(A_1\tau_1 + A_2\tau_2) \quad (2)$$

https://doi.org/10.1021/acsomega.4c07572
ACS Omega 2025, 10, 3486−3493

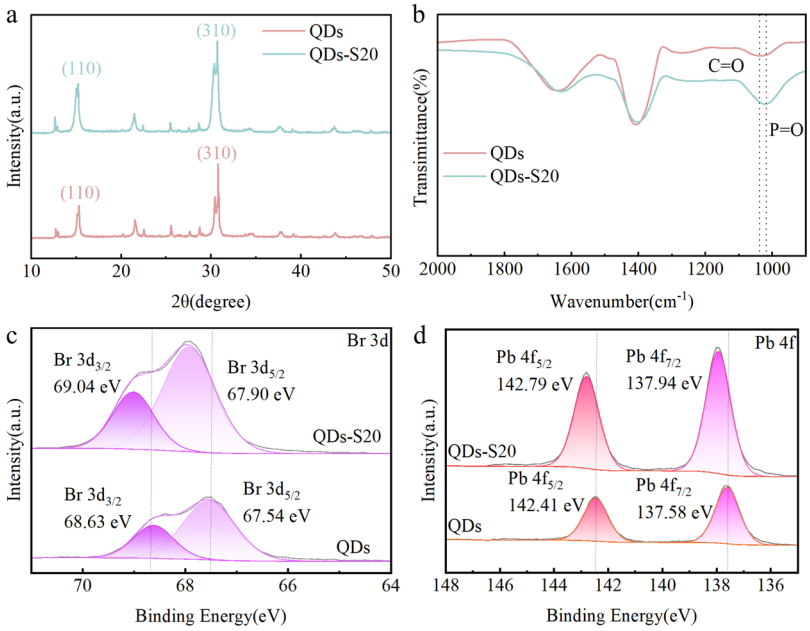

Figure 4. (a, b) XRD and FTIR spectra of QDs and QDS-S20, respectively. (c, d) XPS spectra of Br 3d and Pb 4f, respectively.

2.2. Structural Properties of $CsPbBr_3$. As illustrated in Figure 3a, transmission electron microscopy (TEM) images of perovskites lacking SPE passivation reveal the presence of numerous defects and incomplete crystal structures. It is evident that the core synthesis of the perovskite quantum dots (QDs) is incomplete, exhibiting numerous defects, and the corners of the cubic structure are rounded. In contrast, the perovskites that have undergone SPE passivation (Figure 3b) demonstrate an enhanced QD morphology, marked by sharp corners and uniform surfaces, resulting in a well-defined cubic structure. This observation suggests that the P═O group in SPE coordinates with uncoordinated Pb^{2+}, thereby enhancing the crystal structure and reducing defects.

Figure 3c,d presents high-resolution TEM (HRTEM) images of QDs and QDs-S20, respectively, both displaying well-defined lattice fringes. The lattice fringes of QDs-S20 are more distinct, with interplanar spacings of 2.62 and 4.33 Å, corresponding to the (310) and (110) planes, respectively.

Figures S4 and S5 display the elemental mapping of unpassivated QDs and SPE-passivated QDs, respectively, providing valuable insights into the structural and compositional characteristics of these nanostructures. In the unpassivated QDs, the elements Pb, Cs, Br, and O are identifiable but manifest weak and uneven signals, indicating the presence of crystal defects. In contrast, the SPE-passivated QDs-S20 exhibit stronger and more uniform signals for Pb, Cs, Br, and O, with the P element displaying a distribution trend analogous to those of the other elements. This outcome demonstrates that SPE passivates the perovskite defects uniformly, thereby leading to a more stable structure.

X-ray diffraction (XRD) is a pivotal technique for analyzing the crystal structure and phase composition of materials. The structural changes of $CsPbBr_3$ crystals before and after SPE passivation were investigated through XRD characterization. As illustrated in Figure 4a, the characteristic peaks of the $CsPbBr_3$ crystal at the (110) and (310) crystallographic planes remain unaltered following SPE passivation, thereby aligning with the observed lattice spacing in Figure 3c,d. This observation suggests that the SPE passivation agent does not induce alterations in the crystal structure of $CsPbBr_3$. However, the intensity of the characteristic peaks at the (110) and (310) planes undergoes a substantial increase following SPE passivation. This observation suggests that SPE does not modify the crystal structure of $CsPbBr_3$; rather, it enhances its crystallinity. This observation is consistent with the results obtained from absorption spectroscopy.

Figure 4b presents the Fourier-transform infrared (FTIR) results for the perovskite materials before and after passivation. A comparison of the spectra for unpassivated $CsPbBr_3$ and the passivated samples reveals a significant enhancement of the characteristic peak of the P═O bond at 1021 cm^{-1} after passivation. This observation suggests a robust interaction between the P═O group and the perovskite. In contrast, unpassivated $CsPbBr_3$ displays a characteristic peak at 1053 cm^{-1}, attributed to the carboxyl group (C═O) ligand. Collectively, these observations suggest that SPE enhances the chemical interactions within the perovskite material.

In order to further investigate the interaction between SPE and the perovskite molecules, X-ray photoelectron spectroscopy (XPS) was conducted on the perovskites before and after passivation (see Figures 4c,d, and S6). Following the passivation process, a shift in the binding energies of Br $3d_{3/2}$ and Br $3d_{5/2}$ in QDs-S20 was observed, with an increase from 68.63 to 69.04 eV and from 67.54 to 67.90 eV, respectively. A similar trend is observed in the binding energies of Pb $4f_{5/2}$ and Pb $4f_{7/2}$ in QDs-S20, which increase from 142.41 to 142.79 eV and from 137.58 to 137.94 eV, respectively. These shifts are indicative of enhanced interactions between SPE and the perovskite material. Specifically, the hydroxyl groups, which are formed through the hydrolysis of the ethoxy groups present in the SPE molecule, interact with the Br ions, thereby stabilizing the perovskite structure. Additionally, the binding energies of O 1s increase from 532.20 to 532.45 eV. The peak area of QDs-S20 is 1.22-fold that of QDs. The peak position of O 1s has undergone a shift, accompanied by an increase in the area of the peak. This indicates a change in the oxygen composition of QDs-S20, suggesting the presence of both C═O and P═O

https://doi.org/10.1021/acsomega.4c07572
ACS Omega 2025, 10, 3486−3493

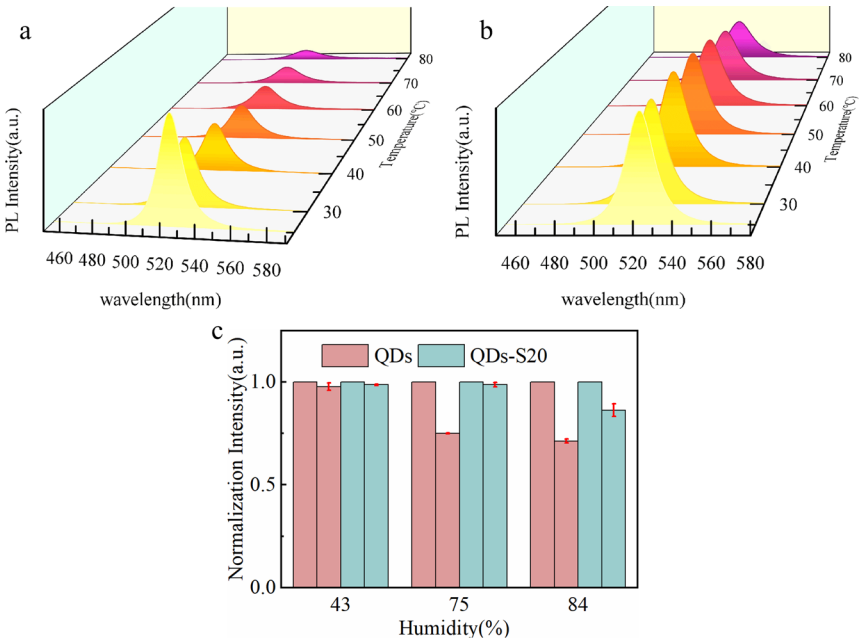

Figure 5. (a, b) Thermal stability test results of QDs and QDS-S20. (c) Relative humidity stability test results.

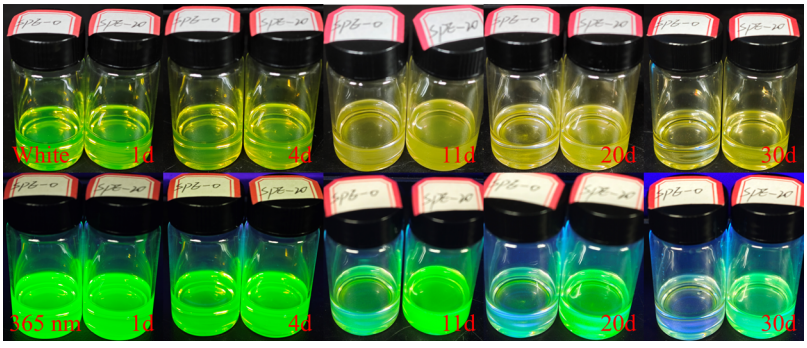

Figure 6. Air stability images of perovskites and passivated perovskites.

bonds in QD-S20 after passivation. The interaction between P═O and Pb^{2+} in QDs-20 has been shown to form a more stable coordination bond, thereby enhancing the binding energy of Pb^{2+}. This process has been demonstrated to reduce the crystal defects of QD-S20 and improve its crystallinity.

2.3. Stability of $CsPbBr_3$. Despite the excellent optoelectronic properties of perovskite QDs, their inherent instability significantly restricts their practical applications.[41] This study explores the alterations in PL intensity of perovskites prior to and following passivation in thermal, humidity, and air environments to assess the stability of the $CsPbBr_3$ materials.

As illustrated in Figure 5a,b, the thermal stability PL spectra of QDs and QDs-S20 reveal a notable difference. QDs-S20 demonstrates a minimal change in PL intensity after heating at 80 °C for 10 min, maintaining 45% of its initial intensity. In contrast, unpassivated QDs demonstrate a substantial decline, reaching only 12% of their initial PL intensity under identical conditions. Moreover, prior to heating, QDs-S20 exhibited a 28% higher PL intensity compared to QDs (Figure 2a), suggesting that the SPE passivation agent not only enhances the optical properties but also improves the thermal stability of $CsPbBr_3$ materials.

Figure 5c presents the humidity stability test results for QDs and QDs-S20. The perovskite solutions were drop-cast onto single-crystal silicon substrates, and after solvent evaporation, the remaining solid perovskites were tested under controlled humidity conditions. At 43% relative humidity (RH), both QDs and QDs-S20 show minimal changes in PL spectra, indicating negligible impact on perovskite stability. However, at 75% RH, QDs-S20 demonstrates nearly unchanged PL intensity, suggesting good humidity stability, whereas unpassivated QDs exhibit a 25% reduction in PL intensity from the initial value. At 84% RH, both QDs and QDs-S20 show reduced PL intensity, but the decrease is less pronounced in QDs-S20, with PL intensity decreasing to 86% of its initial value compared to 71% for QDs. This underscores the superior humidity stability of QDs-S20, attributed to the high chemical stability of the main chain carbon−oxygen−silicon bonds in the SPE molecule, the nonpolar nature of the alkyl side groups providing hydrophobicity, and the overall nonpolar characteristics of the molecule.

Figure 6 illustrates the air stability test results of the perovskites before and after passivation. Initially, there is no significant difference in fluorescence intensity between the two samples, indicating comparable fluorescence properties of the synthesized QDs.

However, by the fourth day, both samples began to exhibit fluorescence quenching, albeit at different rates. Specifically,

https://doi.org/10.1021/acsomega.4c07572
ACS Omega 2025, 10, 3486−3493

QDs-S20 showcases a more gradual quenching process in comparison to QDs. As time progresses, the fluorescence quenching process continues in both samples, with QDs completely losing fluorescence by the twentieth day, while QDs-S20 retains strong fluorescence by the thirtieth day. This outcome demonstrates that passivation significantly enhances the air stability of $CsPbBr_3$ perovskites. The SPE passivation agent interacts with surface traps, vacancies, and dangling bonds on the QDs, thereby reducing nonradiative recombination. Furthermore, the hydrophobic properties imparted by SPE contribute to the enhancement of air stability.

These findings collectively indicate that SPE passivation not only enhances the optical and thermal properties of $CsPbBr_3$ perovskites but also significantly improves their stability under thermal, humid, and air conditions. This advancement renders SPE-passivated perovskites more viable for practical applications.

3. CONCLUSIONS

We successfully synthesized a symmetrical silane passivating agent containing phosphorus−oxygen double bonds. This ionizer has been shown to enhance the optical performance and stability of perovskite QDs. The passivated QDs manifest a substantial enhancement in the PL intensity, PLQY, and average lifetime. Furthermore, passivation enhances the thermal, humidity, and air stabilities of perovskite materials. These findings suggest that the use of phosphorus-containing silane passivators is a promising strategy for enhancing the performance and stability of perovskite-based optoelectronic devices.

4. EXPERIMENTAL SECTION

4.1. Materials. $PbBr_2$ (99.999%), 1,1,3,3-tetramethyldisiloxane (98%), chlorobenzene (99%), oleic acid (OA, 85%), and oleylamine (OAm, 80−90%) were purchased from Macklin. CsBr (99.9%) and DAPP (95%) were purchased from Aladdin. Chloroplatinic acid hexahydrate (99.9%) was obtained from Bidepharm. N,N-Dimethylformamide (DMF, 99.5%), dimethyl sulfoxide (DMSO, 99.5%), ethyl acetate (99.5%), and hexane (99.5%) were purchased from Sinopharm Chemical Reagent. All of the reagents were used without further purification.

4.2. Synthesis of SPE Passivator. To prepare the SPE passivator, 0.74 mL of 1,1,3,3-tetramethyldisiloxane, 1.4 mL of DAPP, and 0.01 g of chloroplatinic acid hexahydrate were added to a 10 mL round-bottom flask. The mixture was stirred in an ice−water bath under a nitrogen atmosphere for 1 h. Following this, an additional 1 mL of 1,1,3,3-tetramethyldisiloxane was added in two separate portions, and the reaction was continued under the same conditions for another hour. After completion of the reaction, 30 mL of hexane was introduced into the reaction mixture, which was stirred at room temperature for 30 min and allowed to stand for 2 h. The mixture was then centrifuged at 8000 rpm for 3 min. The supernatant was subjected to reduced-pressure distillation at 20 °C. The final product, a pale yellow liquid, was identified as the SPE passivator.

4.3. Synthesis of $CsPbBr_3$ Quantum Dots. To synthesize the $CsPbBr_3$ perovskite QDs, 0.2 mmol of $PbBr_2$, 0.2 mmol of CsBr, 3.5 mL of DMF, 1.5 mL of DMSO, 0.25 mL of OAm, and 0.5 mL of OA were combined in a 20 mL sample vial and stirred at room temperature for 24 h to form the precursor solution. Subsequently, 5 mL of chlorobenzene was introduced into the reactor, and the stirring rate was elevated to a high-speed vortex setting. Then, 0.2 mL of the precursor solution was added to the reactor, and stirring continued vigorously for 20 s. The mixture was centrifuged at 8000 rpm for 3 min, and the precipitate was collected to yield the $CsPbBr_3$ QDs, referred to as QDs.

4.4. Synthesis of SPE-Passivated Perovskites. During the preparation of the precursor solution, the other raw materials remained unchanged, while the SPE passivator was used at concentrations of 5, 10, 20, and 30 mg/mL. The subsequent steps followed the same procedure as those for the synthesis of QDs. The resulting QDs were labeled as QDs-S5, QDs-S10, QDs-S20, and QDs-S30, respectively.

4.5. Characterization. This work employs characterization methods, including PL spectra, UV−vis absorption spectra, PLQY, TRPL, TEM, scanning electron microscopy, energy-dispersive spectrometry, XRD, FTIR, XPS, NMR, thermal stability test, humidity stability test, and air stability test. The detailed information about the above characterization is presented in the Supporting Information.

■ ASSOCIATED CONTENT

Supporting Information

The Supporting Information is available free of charge at https://pubs.acs.org/doi/10.1021/acsomega.4c07572.

Experimental section, SPE synthesis route, NMR, Urbach energy calculation process, elemental mapping, and TRPL fitting parameters (PDF)

■ AUTHOR INFORMATION

Corresponding Author

Chuanhua Gao − *College of Chemical and Material Engineering, Quzhou University, Quzhou 324000, China; Department of Chemical and Materials Engineering, The University of Auckland, Auckland 1010, New Zealand;* orcid.org/0009-0003-0623-4473; Email: chuanhua_gao@aliyun.com

Authors

Baoyang Dai − *College of Chemical and Material Engineering, Quzhou University, Quzhou 324000, China; College of Chemical Engineering, Zhejiang University of Technology, Hangzhou 310014, China*

Shanshan Yan − *College of Chemical and Material Engineering, Quzhou University, Quzhou 324000, China*

Zhimi Chen − *College of Chemical and Material Engineering, Quzhou University, Quzhou 324000, China; College of Chemical Engineering, Zhejiang University of Technology, Hangzhou 310014, China*

Tucai Zheng − *College of Chemical and Material Engineering, Quzhou University, Quzhou 324000, China*

Jie Qin − *College of Chemical and Material Engineering, Quzhou University, Quzhou 324000, China*

Junhua Zhao − *College of Chemical and Material Engineering, Quzhou University, Quzhou 324000, China*

Wanting Jin − *College of Chemical and Material Engineering, Quzhou University, Quzhou 324000, China*

Chunhui Zhou − *College of Chemical Engineering, Zhejiang University of Technology, Hangzhou 310014, China;* orcid.org/0000-0001-5733-9011

https://doi.org/10.1021/acsomega.4c07572
ACS Omega 2025, 10, 3486−3493

Li Wan − *Department of Chemical and Materials Engineering, The University of Auckland, Auckland 1010, New Zealand*
Xing Su − *College of Chemical and Material Engineering, Quzhou University, Quzhou 324000, China*

Complete contact information is available at: https://pubs.acs.org/10.1021/acsomega.4c07572

Author Contributions

B.D. and C.G. conceived the study. B.D., S.Y., Z.C., and T.Z. designed and performed the experiments. B.D. performed TEM and XRD characterization, Z.C. and W.J. helped with stability testing and analysis. J.Q. helped with nuclear magnetic spectrum and analysis. J.Z. helped calculate the Urbach energy. C.Z. helped to revise the sentences of the whole article. L.W. and X.S. helped with TEM analysis. B.D. and C.G. wrote the manuscript with input from all the authors. All authors reviewed the final manuscript.

Notes

The authors declare no competing financial interest.

■ ACKNOWLEDGMENTS

We gratefully acknowledge the financial support from the National Natural Science Foundation of China (Grant No. 52103086), the Joint Funds of the Zhejiang Provincial Natural Science Foundation of China (Grant Nos. LZY22E030001and LZY24H160001), and the Basic Research Plan for Public Welfare of Zhejiang Province of China (Grant No. LZY21B060001).

■ REFERENCES

(1) Karlsson, M.; Yi, Z.; Reichert, S.; Luo, X.; Lin, W.; Zhang, Z.; Bao, C.; Zhang, R.; Bai, S.; Zheng, G.; Teng, P.; Duan, L.; Lu, Y.; Zheng, K.; Pullerits, T.; Deibel, C.; Xu, W.; Friend, R.; Gao, F. Mixed halide perovskites for spectrally stable and high-efficiency blue light-emitting diodes. *Nat. Commun.* **2021**, *12* (1), 361.
(2) Hoang, M. T.; Pannu, A. S.; Yang, Y.; Madani, S.; Shaw, P.; Sonar, P.; Tesfamichael, T.; Wang, H. Surface Treatment of Inorganic $CsPbI_3$ Nanocrystals with Guanidinium Iodide for Efficient Perovskite Light-Emitting Diodes with High Brightness. *Nano-Micro Lett.* **2022**, *14* (1), 69.
(3) Tseng, Z.-L.; Chen, S.-A.; Uma, K.; Chen, Y.-S.; Ke, K.-Y.; Xie, J.-X.; Chiang, C. Y. All-solution-processed perovskite-quantum-dot light-emitting diodes through effective synergistic combination of orthogonal solvent and electron transport material. *Alex. Eng. J.* **2024**, *97*, 256−266.
(4) Luo, D.; Zhao, L.; Wu, J.; Hu, Q.; Zhang, Y.; Xu, Z.; Liu, Y.; Liu, T.; Chen, K.; Yang, W.; Zhang, W.; Zhu, R.; Gong, Q. Dual-Source Precursor Approach for Highly Efficient Inverted Planar Heterojunction Perovskite Solar Cells. *Adv. Mater.* **2017**, *29* (19), No. 1604758.
(5) Zhang, S.; Ye, F.; Wang, X.; Chen, R.; Zhang, H.; Zhan, L.; Jiang, X.; Li, Y.; Ji, X.; Liu, S.; Yu, M.; Yu, F.; Zhang, Y.; Wu, R.; Liu, Z.; Ning, Z.; Neher, D.; Han, L.; Lin, Y.; Tian, H.; Chen, W.; Stolterfoht, M.; Zhang, L.; Zhu, W.-H.; Wu, Y. Minimizing buried interfacial defects for efficient inverted perovskite solar cells. *Science* **2023**, *380* (6643), 404−409.
(6) Tang, H.; Shen, Z.; Shen, Y.; Yan, G.; Wang, Y.; Han, Q.; Han, L. Reinforcing self-assembly of hole transport molecules for stable inverted perovskite solar cells. *Science* **2024**, *383* (6688), 1236−1240.
(7) Jiang, Q.; Zhao, Y.; Zhang, X.; Yang, X.; Chen, Y.; Chu, Z.; Ye, Q.; Li, X.; Yin, Z.; You, J. Surface passivation of perovskite film for efficient solar cells. *Nat. Photonics* **2019**, *13* (7), 460−466.
(8) Wang, H.; Kim, D. H. Perovskite-based photodetectors: materials and devices. *Chem. Soc. Rev.* **2017**, *46* (17), 5204−5236.
(9) Niu, G.; Guo, X.; Wang, L. Review of recent progress in chemical stability of perovskite solar cells. *J. Mater. Chem. A* **2015**, *3* (17), 8970−8980.
(10) Wang, L.; Zhou, H.; Hu, J.; Huang, B.; Sun, M.; Dong, B.; Zheng, G.; Huang, Y.; Chen, Y.; Li, L.; Xu, Z.; Li, N.; Liu, Z.; Chen, Q.; Sun, L.-D.; Yan, C.-H. A Eu^{3+}-Eu^{2+} ion redox shuttle imparts operational durability to Pb-I perovskite solar cells. *Science* **2019**, *363* (6424), 265−270.
(11) Liu, W.; Feng, Y.; Li, L.; Ma, Y.; Hu, R.; Wu, X.; Chu, L.; Li, X. A.; Huang, W. Stable and Efficient Pb-Ni Binary Metal Perovskite Solar Cells. *Acs Sustain. Chem. Eng.* **2021**, *9* (50), 17112−17119.
(12) Zhao, Y.; Ma, F.; Qu, Z.; Yu, S.; Shen, T.; Deng, H.-X.; Chu, X.; Peng, X.; Yuan, Y.; Zhang, X.; You, J. Inactive $(PbI_2)_2$ > RbCl stabilizes perovskite films for efficient solar cells. *Science* **2022**, *377* (6605), 531−534.
(13) Zhuang, Q.; Zhang, C.; Gong, C.; Li, H.; Li, H.; Zhang, Z.; Yang, H.; Chen, J.; Zang, Z. Tailoring multifunctional anion modifiers to modulate interfacial chemical interactions for efficient and stable perovskite solar cells. *Nano Energy* **2022**, *102*, No. 107747.
(14) Gu, L.; Chen, M.; Liu, X.; Chen, D.; Gu, Y.; Wang, S. Halogen Anion Management in Solution-Processed Perovskite Films for Efficient Solar Cells. *Sol. RRL* **2024**, *8* (6), No. 2301001.
(15) Gu, X.; Xiang, W.; Tian, Q.; Liu, S. Rational Surface-Defect Control via Designed Passivation for High-Efficiency Inorganic Perovskite Solar Cells. *Angew. Chem., Int. Ed.* **2021**, *60* (43), 23164−23170.
(16) Zhao, W.; Xu, J.; He, K.; Cai, Y.; Han, Y.; Yang, S.; Zhan, S.; Wang, D.; Liu, Z.; Liu, S. A Special Additive Enables All Cations and Anions Passivation for Stable Perovskite Solar Cells with Efficiency over 23%. *Nano-Micro Lett.* **2021**, *13* (1), 169.
(17) Cho, S.-P.; Lee, H.-J.; Seo, Y.-H.; Na, S.-I. Multifunctional passivation agents for improving efficiency and stability of perovskite solar cells: Synergy of methyl and carbonyl groups. *Appl. Surf. Sci.* **2022**, *575*, No. 151740.
(18) Wang, P.; Liu, J.; Shang, W.; Xu, T.; Wang, M.; Shi, Y.; Cai, R.; Bian, J. Rational Selection of the Lewis Base Molecules Targeted for Lead-Based Defects of Perovskite Solar Cells: The Synergetic Co-passivation of Carbonyl and Carboxyl Groups. *J. Phys. Chem. Lett.* **2023**, *14* (3), 653−662.
(19) Li, L.; Tu, S.; You, G.; Cao, J.; Wu, D.; Yao, L.; Zhou, Z.; Shi, W.; Wang, W.; Zhen, H.; Ling, Q. Enhancing performance and stability of perovskite solar cells through defect passivation with a polyamide derivative obtained from benzoxazine-isocyanide chemistry. *Chem. Eng. J.* **2022**, *431*, No. 133951.
(20) Wang, M.; Zhao, Y.; Jiang, X.; Yin, Y.; Yavuz, I.; Zhu, P.; Zhang, A.; Han, G. S.; Jung, H. S.; Zhou, Y.; Yang, W.; Bian, J.; Jin, S.; Lee, J.-W.; Yang, Y. Rational selection of the polymeric structure for interface engineering of perovskite solar cells. *Joule* **2022**, *6* (5), 1032−1048.
(21) Zhang, L.; Gao, J.; You, Z.; Li, Q.; Liu, M.; Ma, Z.; Liu, Y. A multifunctional phosphorylcholine-based polymer reduces energy loss for efficient perovskite solar cells. *J. Mater. Chem. C* **2022**, *10* (44), 16781−16788.
(22) Jiao, Y.; Yao, X.; Bao, F.; Mao, J.; Chen, H.; Duan, Y.; Yang, P.; Tang, Q.; He, B. Crystallization Regulation and Dual-Defects Healing by Self-Polymerization of Multifunctional Monomer Additives for Stable and Efficient $CsPbBr_3$ Perovskite Solar Cells. *Sol. RRL* **2023**, *7* (3), No. 2200883.
(23) Jeong, J.; Kim, M.; Seo, J.; Lu, H.; Ahlawat, P.; Mishra, A.; Yang, Y.; Hope, M. A.; Eickemeyer, F. T.; Kim, M.; Yoon, Y. J.; Choi, I. W.; Darwich, B. P.; Choi, S. J.; Jo, Y.; Lee, J. H.; Walker, B.; Zakeeruddin, S. M.; Emsley, L.; Rothlisberger, U.; Hagfeldt, A.; Kim, D. S.; Graetzel, M.; Kim, J. Y. Pseudo-halide anion engineering for α-$FAPbI_3$ perovskite solar cells. *Nature* **2021**, *592* (7854), 381−385.
(24) Zhang, P.; Gu, N.; Chen, X.; Song, L.; Du, P.; Chen, W.-H.; Xiong, J. Triethyl phosphate in an antisolvent: a novel approach to fabricate high-efficiency and stable perovskite solar cells under ambient air conditions. *Mater. Chem. Front.* **2021**, *5* (20), 7628−7637.
(25) Lee, Y. S.; Jung, J. W. A functionalized phosphorous tetrabenzotriazacorrole dye as a novel passivating agent of high-

performance planar perovskite solar cells. *J. Alloys Compd.* **2023**, *960*, No. 171015.
(26) Wu, J.; Li, M.-H.; Jiang, Y.; Xu, Q.; Xian, L.; Guo, H.; Wan, J.; Wen, R.; Fang, Y.; Xie, D.; Lei, Y.; Hu, J.-S.; Lin, Y. Carrier Management via Integrating InP Quantum Dots into Electron Transport Layer for Efficient Perovskite Solar Cells. *ACS Nano* **2022**, *16* (9), 15063−15071.
(27) Bao, C.; Yang, J.; Bai, S.; Xu, W.; Yan, Z.; Xu, Q.; Liu, J.; Zhang, W.; Gao, F. High Performance and Stable All-Inorganic Metal Halide Perovskite-Based Photodetectors for Optical Communication Applications. *Adv. Mater.* **2018**, *30* (38), No. e1803422.
(28) Cheng, C.; Yao, Y.; Li, L.; Zhao, Q.; Zhang, C.; Zhong, X.; Zhang, Q.; Gao, Y.; Wang, K. A Novel Organic Phosphonate Additive Induced Stable and Efficient Perovskite Solar Cells with Efficiency over 24% Enabled by Synergetic Crystallization Promotion and Defect Passivation. *Nano Lett.* **2023**, *23* (19), 8850−8859.
(29) Wang, Z.; Gao, H.; Wu, D.; Meng, J.; Deng, J.; Cui, M. Defects and Defect Passivation in Perovskite Solar Cells. *Molecules* **2024**, *29* (9), 2104.
(30) Shen, X.; Lin, X.; Peng, Y.; Zhang, Y.; Long, F.; Han, Q.; Wang, Y.; Han, L. Two-Dimensional Materials for Highly Efficient and Stable Perovskite Solar Cells. *Nano-Micro Lett.* **2024**, *16* (1), 201.
(31) Lee, G. H.; Kim, K.; Kim, Y.; Yang, J.; Choi, M. K. Recent Advances in Patterning Strategies for Full-Color Perovskite Light-Emitting Diodes. *Nano-Micro Lett.* **2024**, *16* (1), 45.
(32) Jeon, S. O.; Lee, J. Y. Phosphine oxide derivatives for organic light emitting diodes. *J. Mater. Chem.* **2012**, *22* (10), 4233−4243.
(33) Li, L.; Wang, Y.; Wang, X.; Lin, R.; Luo, X.; Liu, Z.; Zhou, K.; Xiong, S.; Bao, Q.; Chen, G.; Tian, Y.; Deng, Y.; Xiao, K.; Wu, J.; Saidaminov, M. I.; Lin, H.; Ma, C.-Q.; Zhao, Z.; Wu, Y.; Zhang, L.; Tan, H. Flexible all-perovskite tandem solar cells approaching 25% efficiency with molecule-bridged hole-selective contact. *Nature Energy* **2022**, *7* (8), 708−717.
(34) Li, R.; Jing, Y.; Liu, X.; Xu, Y.; Wang, D.; Li, W.; Hou, W.; Wu, J.; Lan, Z. Stability enhancement of perovskite solar cells via multi-point ultraviolet-curing-based protection. *J. Power Sources* **2022**, *520*, No. 230906.
(35) Mehdizadeh-Rad, H.; Singh, J. Influence of Urbach Energy, Temperature, and Longitudinal Position in the Active Layer on Carrier Diffusion Length in Perovskite Solar Cells. *ChemPhysChem* **2019**, *20* (20), 2712−2717.
(36) Subedi, B.; Li, C. W.; Chen, C.; Liu, D. C.; Junda, M. M.; Song, Z. N.; Yan, Y. F.; Podraza, N. J. Urbach Energy and Open-Circuit Voltage Deficit for Mixed Anion-Cation Perovskite Solar Cells. *ACS Appl. Mater. Interfaces* **2022**, *14* (6), 7796−7804.
(37) Wang, Z.; Wei, Y.; Chen, Y.; Zhang, H.; Wang, D.; Ke, J.; Liu, Y.; Hong, M. "Whole-Body" Fluorination for Highly Efficient and Ultra-Stable All-Inorganic Halide Perovskite Quantum Dots. *Angew. Chem., Int. Ed.* **2024**, *63* (8), No. e202315841.
(38) Yang, D.; Li, X.; Wu, Y.; Wei, C.; Qin, Z.; Zhang, C.; Sun, Z.; Li, Y.; Wang, Y.; Zeng, H. Surface Halogen Compensation for Robust Performance Enhancements of $CsPbX_3$ Perovskite Quantum Dots. *Adv. Opt. Mater.* **2019**, *7* (11), No. 1900276.
(39) Shi, J.; Deng, H.; Liu, F.; Li, R.; Qiu, X.; Tu, Y.; Wu, L.; Xu, Y.; Tian, J.; Zhu, C.; Wu, J.; Lan, Z. Polar Species Modified Dielectric Constant of $CsPbI_2Br$ Perovskite Nanocrystals: Implications for Carbon-Based Perovskite Solar Cells. *Acs Appl. Nano Mater.* **2024**, *7* (12), 14363−14371.
(40) Ghosh, S.; Pradhan, B.; Lin, W.; Zhang, Y.; Leoncino, L.; Chabera, P.; Zheng, K.; Solano, E.; Hofkens, J.; Pullerits, T. Slower Auger Recombination in 12-Faceted Dodecahedron $CsPbBr_3$ Nanocrystals. *J. Phys. Chem. Lett.* **2023**, *14* (4), 1066−1072.
(41) Zhang, Y.; Chouhan, L.; Fron, E.; Leoncino, L.; Elkhouly, K.; Bhatia, H.; Qiu, W.; Roeffaers, M. B. J.; Hofkens, J.; Debroye, E.; Pradhan, B. Operationally Stable and Efficient $CsPbI_{3-x}Br_x$ Perovskite Nanocrystal Light-Emitting Diodes Enabled by Ammonium Ligand Surface Treatment. *ACS Photonics* **2023**, *10* (8), 2774−2783.38.

https://doi.org/10.1021/acsomega.4c07572
ACS Omega 2025, 10, 3486−3493